8-27-2012

3D ICEPIC simulations of pulsed relativistic magnetron with transparent cathode : a comparative study with 3D MAGIC simulations

Cassandra Mendonca

3D ICEPIC SIMULATIONS OF A6 RELATIVISTIC MAGNETRON WITH TRANSPARENT CATHODE: A COMPARATIVE STUDY WITH MAGIC SIMULATIONS

by

CASSANDRA MENDONCA

BACHELORS OF SCIENCE

THESIS

Submitted in Partial Fulfillment of the

Requirements for the Degree of

Masters of Science
Electrical Engineering

The University of New Mexico

Albuquerque, New Mexico

July, 2012

Cassandra Mendonca

Candidate

Electrical and Computer Engineering

Department

This thesis is approved, and it is acceptable in quality and form for publication:

Approved by the Thesis Committee:

Edl Schamiloglu , Chairperson

Timothy Fleming

Sarita Prasad

Mark Gilmore

DEDICATION

I dedicate this thesis to my son, Richard, my true inspiration. You have been there the whole way. I love you.

ACKNOWLEDGMENTS

This Thesis would not have been possible without all the help and support of all the kind and talented people around me. I would never have made it through the process without all the guidance from my advisor, committee members, friends and family members. I don't know if everyone realizes how personal this accomplishment has been for me but coming all the way from where I was at has been one of the greatest journeys in my life.

I want to give my deepest gratitude to Professor Edl Schamiloglu, my advisor and chair, for all the years of teaching, all the years of advisement, and all the years of inspiration. You have been there through thick and thin and never once told me I would not make it. Sometimes I thought I would not make it another day and you would remind to get right back on track and move forward. Thank you for that. You have guided me through this degree with inspiration, support, and knowledge. I have been so honored to be part of your Applied EM group to be surrounded by such smart talented people.

I want to give special thanks to my mentors Dr. Sarita Prasad (UNM) and Timothy Fleming (AFRL) without the immeasurable knowledge and expertise this thesis would not have been possible. Thank you to both of you for all your patience, understanding and guidance. I have learned so much and have been privileged to have worked with you two.

I also want to thank all fellow graduate students who have made coming to school over the years fun and exciting. Thanks to Shawn Soh and Christopher Leach for all the

help with my classes, without the team work classes would have been seriously missing something .

Thanks to my family for putting up with all my many years of schooling. Without all the support I would not have made it. Some day it will be my turn. Thanks dad I know I owe you big time. Richard son I love you so much.

3D ICEPIC Simulation of A6 Magnetron with Transparent Cathode: A Comparative Study with MAGIC Simulations

By Cassandra Mendonca

B.S., Electrical Engineering, University of New Mexico, 2007

M.S., Electrical Engineering, University of New Mexico 2012

Abstract

Ongoing research at the University of New Mexico (UNM) shows significant improvement in the start time and rate of build-up of microwave oscillations in a relativistic magnetron that uses a transparent cathode. In recent studies conducted at UNM the experimental results and the results of numerical simulations using the 3-dimensional particle-in-cell (PIC) code MAGIC have shown strong correlation.

For this research a 3-dimensional PIC code ICEPIC developed at the Air Force Research Laboratory (AFRL) was used to simulate the A6 magnetron geometry with a transparent cathode. The results were compared with the work done at UNM to test the fidelity of the two simulation codes. Output parameters such as microwave power, microwave frequency, anode current, and leakage current with respect to the axial magnetic field were compared.

ICEPIC simulations were run on a parallel architecture with 64 CPUs at a grid resolution of 1mmx 1mmy 1mmz in the 3-dimensional Cartesian coordinate system. These simulations consisted of roughly 6 million active grid cells and 16 million

particles. Results indicated agreement between results from ICEPIC and MAGIC to within 20% for standard performance parameters. ICEPIC simulations also confirmed oscillation of the A6 magnetron with transparent cathode at 4 GHz in the 2π-mode.

Table of Contents

Chapter 1

Introduction

Background

Albert W. Hull of General Electric Research Laboratory invented the original magnetron while searching for an alternative to the vacuum-tube diode in 1916. In the early 1920's it was demonstrated that the magnetron could be used at low frequencies as an amplifier or oscillator in radio systems. In the mid 1920's independently in Europe and Japan the idea of very-high-frequency oscillations in magnetrons was studied. Around this same time the electrophysicst Hidesugu Yagi demonstrated that relatively short waves could be used for point-to-point communications. Also, during this research it was discovered that the presence of ships and airplanes could be detected by reflected energy from the magnetron. This sparked ideas and the inherent deficiencies of existing vacuum tubes at the time made magnetrons an attractive alternative for use in radio detection systems.

Increasing concern over German bombers during World War II created an urgent need for more powerful sources of microwave energy, which provided the stimulus for the invention of the cavity magnetron. Boot and Randall, who were members of the microwave group at the University of Birmingham, visited a radar installation and after learning how the systems operated came up with the idea of the cavity resonator. The various design investigations in the late 1930's and better understanding of cavity resonators led to the first successful high power magnetron experiment on February 21,

1940 by Randall and Boot. By May of that same year a radar system using Randall and Boot's design was successful in detecting a submarine telescope 7 miles away. By October 6, 1940 an 8-cavity magnetron was demonstrated at Bell Telephone Laboratories. The tube produced 10 cm wavelength radiation at10 kW power levels [1].

By the end of World War II magnetrons were capable of pulsing 3 MW of power in the S-band frequency range with 60% efficiency. It was said that the magnetron was the decisive factor of the war. Radar changed to war for our side and the magnetron has been said to be one of the greatest inventions of the 20th century. Since 1945 further advances in pulsed power magnetrons have been less frequent due to the difficulty in understanding of the theory of microwave circuits. The reason for this lack of progress is due to the fact that magnetron development relied heavily on empirical design rather than theoretical results. The nonlinear 2-D kinetic properties of the magnetron do not readily lend themselves to a self-consistent mathematical analysis. Today magnetrons are considered one of the most efficient high power microwave (HPM) sources; however; they are not ideal for short pulse applications [2].

High power microwave (HPM) devices are necessary for a number of applications including radar and communications. The relativistic magnetron is one of the most compact, powerful, and agile HPM sources available today. These devices are capable of high output power (GW-class) with applications over a wide range of frequencies. However, for applications where short pulse high peak power is desired, the relativistic magnetron, equipped with a traditional solid cathode, has several performance deficiencies. Among them are the start time of oscillation, the rate at which oscillations build-up, mode competition and finally the RF output power and efficiency. The non-

relativistic magnetron has operated at efficiencies of nearly 90%, whereas the relativistic magnetron, however, has operated with efficiency in the range of about 30% [3].

1.2 Thesis Outline

This thesis describes the results of ICEPIC simulations comparing and contrasting the MAGIC simulations of the transparent cathode-driven A6 magnetron performed at UNM. The remainder of this thesis is organized as follows: Chapter 1 discusses an introduction and brief history of the Relativistic Magnetron. Chapter 2 discusses the theory of magnetron operation, discussing design parameters, the Buneman-Hartree condition, and magnetron operation with a solid cathode. Chapter 3 discusses the software including a brief description of the 3D code MAGIC. The focus of Chapter 3 is to provide a software description of ICEPIC, such as the YEE algorithm, parallel processing, particles, and grid set-up. We discuss simulation diagnostics for voltage, current, magnetic field, power, extraction port, and the permanently matched layer (PML) boundary condition. Chapter 4 discusses simulation results, which include the grid set-up for simulations of the A6 magnetron with a transparent cathode and graphs that include the results for voltage, power, magnetic field, mode selection, anode current, and leakage current. These results are compared with MAGIC simulation results. Chapter 5 presents a summary of this thesis and recommendations for future work.

Chapter 2

Physics of Magnetron Operation

2.1 Physics of Magnetron Operation

The relativistic magnetron shown in Fig. 2.1 is capable of producing power on the order of 1 GW. A radial electric field is applied between the coaxial anode and cathode in the presence of a magnetic field. In the anode cathode (A-K) gap electrons are emitted from the cathode and execute an ExB azimuthal drift attributed to the radial electric field (E) crossed with the axial magnetic field (B). Resonators in the anode block form a slow wave structure and support RF modes which can interact with the electron drift when there is synchronism between the phase velocity of an RF mode and the drift velocity of electrons. At this resonance the wave-particle interaction is such that electrons convert their energy to the RF mode that couples out of the resonator, usually through a narrow slot at one or more of the cavities.

As electrons are emitted from the cathode they perform an azimuthal drift only if the magnitude of the axial magnetic is sufficient to insulate the electrons. The critical value of the axial magnetic field for which the electron trajectory is purely azimuthal at the anode radius is called the cutoff magnetic field, B_z=B* and is expressed in Eq. 2.1. This is called the Hull cut-off condition.

$$B^* = \frac{mc}{q\, d_e}\left[\left(\frac{2qV}{mc^2}\right) + \left(\frac{qV}{mc^2}\right)^2\right]^{1/2} \qquad \text{(Equation 2.1)}$$

In Eq. 2.1 m is the electron mass, q is the electron charge, c is the speed of light, d_e is the A-K gap spacing, and V is the voltage. Three assumptions were used in deriving Eq. 2.1:

1. The geometry is assumed to be smooth
2. electrons leave the cathode with zero initial velocity
3. all fields are constant in time.

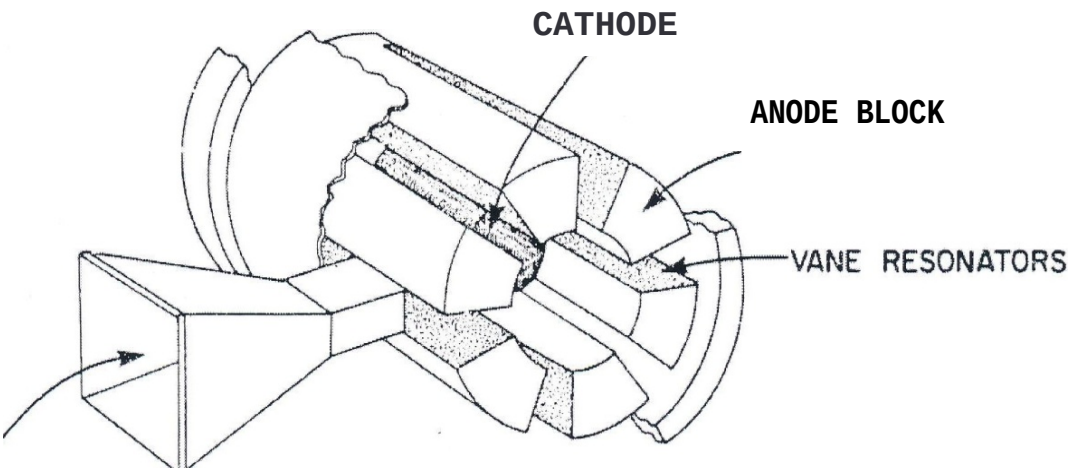

Figure 2.1. Schematic of a relativistic magnetron [2].

At the Hull cut-off condition stated, electrons emitted from the cathode with zero initial velocity reach the anode with the radial component of their velocity equal to zero. For $B_z<B^*$ at a given voltage electrons are not insulated and current is drawn across the

gap. Under perfect magnetic insulation steady state can occur. The most common steady state solutions are “double stream” in which electrons have cycloidol motion and “single stream" here electrons move parallel to the electrode surfaces. The state in which electrons move parallel to the electrode with drift velocity v = ExB/ | B | ^{2} is known as the “Brillouin flow” condition. Results here show both solutions, a mixture of “double stream” and “single stream,” so this steady-state is not stable.

The interaction space and resonator vanes can be thought of as a cavity resonator that has an infinite number of modes where some modes have velocities less than the speed of light. When there is a synchronism between the velocity of the RF wave and the electron drift, a wave-particle interaction occurs. As this wave-particle interaction occurs the RF wave can alter the trajectories of the particles, allowing the particles to cross the A-K gap. The DC potential energy loss while crossing the gap is qV. If the increase in kinetic energy of the electron is less than qV then by conservation of energy the balance is given up to the RF wave. As B_z increases such that Bz > B* the drift velocity will decrease and electrons in the outermost part of the space charge layer will no longer move in synchronism and oscillations will no longer exist. The magnetic field B_{BH} for which this happens is known as the Buneman-Harteee condition. The oscillation frequency is f_n, n is the number of vanes, and r_a and r_c and the anode and cathode radii, respectively.

$$\frac{qV}{mc^2} = \left(\frac{q\,B_{BH}}{mc}\right)\left(\frac{2\pi f_n r_a}{nc}\right)\left(\frac{r_a^2 - r_c^2}{2r_a}\right) - \left\{1 - \left[1 - \left(\frac{2\pi f_n r_a}{nc}\right)^2\right]^{1/2}\right\} \qquad (2.2)$$

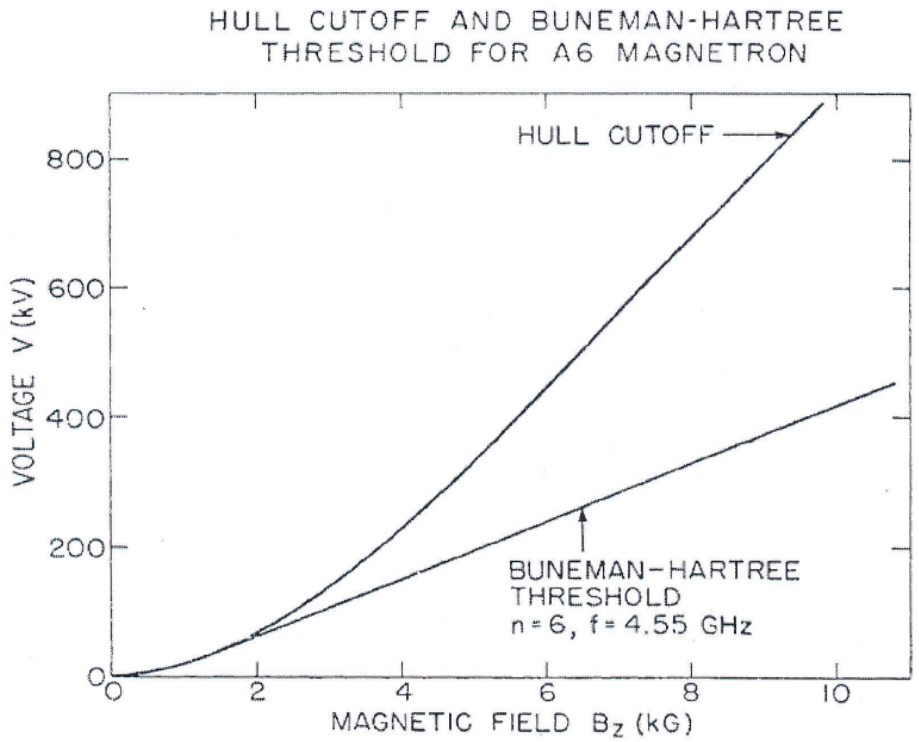

Figure 2.2. Hull cut-off and Buneman-Hartree condition for the A6 magnetron [2].

2.2 The A6 Magnetron Design Parameters

The A6 magnetron, developed at MIT, was the first relativistic magnetron capable of producing power in the 100's of MW range with frequency in the S-Band. Voltages were applied at the MV level, in contrast with conventional magnetrons with applied voltages in the kV range. Another characteristic parameter of the MIT A6 magnetron is the use of field emission cathodes capable of drawing 100's kA of current. The pulse length of the relativistic magnetron is only constrained by the limitation of the pulsed power driver.

While the efficiency of conventional magnetrons is 50% or greater, the efficiencies of the relativistic magnetron are steady at approximately 20%.

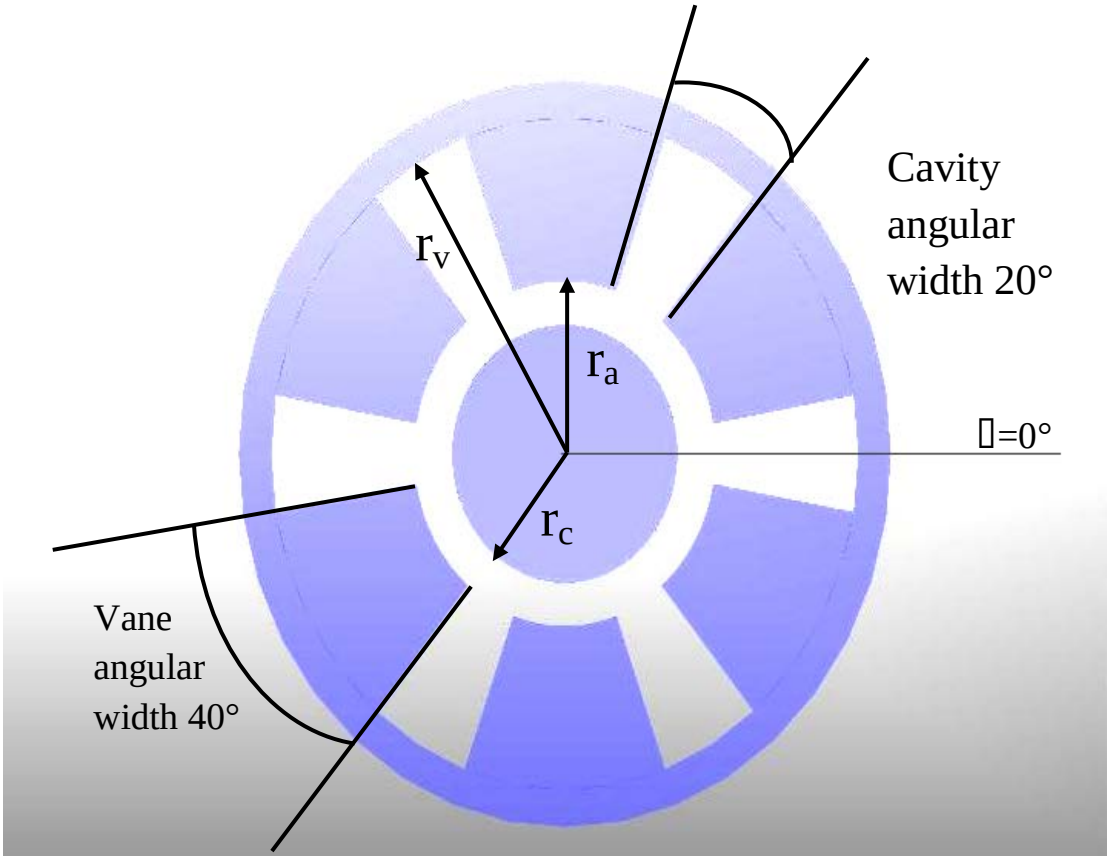

Figure 2.3. Axial view of the A6 relativistic magnetron with a solid cathode.

The character dimensions for the MIT A6 magnetron with solid cathode are as follows:

r_c = cathode radius
r_a = anode radius
r_v = radius of vane resonators

r_c = 1.58 cm
r_a = 2.11 cm
r_v = 4.11 cm

N = number of resonators
L = length of magnetron in meters
π mode is 2.34 GHz, 2π mode is 4.60 GHz

N = 6
L = 0.072 m
π mode is 2.34 GHz, 2π mode is 4.60 GHz

The operating modes for a magnetron are TE modes with an RF field entirely axial in the z-direction. To calculate the frequency of the modes of oscillation, analytically, one must solve Maxwell's equations with two assumptions: first the cathode and anode are infinitely long in the z-direction making the problem two dimensional and second, neglect space charge. The solutions are generated by solving for the interaction space and the resonators separately. The RF admittance of both solutions is then set equal to each other, which results in a transcendental equation for the given frequencies. Implicit in this solution, also, is that the electric field across the A-K gap is constant, which is not met in the limit of narrow vanes [2].

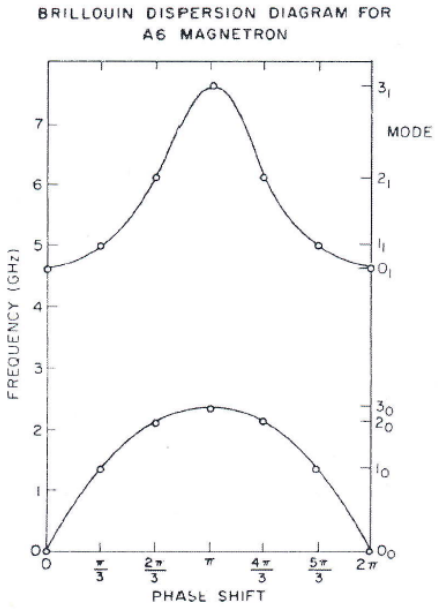

Figure 2.4. Dispersion diagram for the MIT A6 magnetron [2].

Figure 2.4 is the dispersion relation for Brillouin flow. The A6 MIT magnetrons' preferred operating mode is the 2π mode with all of the RF fields in the resonator in phase [2].

In our initial work we carried out simulations in ICEPIC with the exact dimensions and design parameters for the A6 MIT magnetron. Since there is plentiful data for the A6 MIT magnetron with a solid cathode we used this as a starting point. We initially ran simulations with the solid cathode as a means to gauge our input coding.

Chapter 3

Cathode Priming and Transparent Cathode

Research at the University of New Mexico (UNM) and the University of Michigan (UM) has been directed at performance improvements in output power, efficiency, and mode purity in relativistic magnetrons. One technique that has demonstrated magnetron performance improvement is priming, which includes magnetic priming, cathode priming, and electrostatic priming.

3.1 Cathode Designs for Priming Techniques

For pulsed-power-driven magnetrons the driving power is only available to the magnetron for ten to a few hundred nanoseconds so in order to utilize the energy the magnetron needs to operate in the desired mode as quickly as possible. This has been an area of considerable study because magnetrons are notoriously slow when it comes to the time it takes for the oscillations to start-up. Oscillations start from noise, which is not a very efficient way to start oscillations. Researchers at UNM, UM, and the Air Force Research Laboratory, Kirtland Air Force Base (AFRL) have studied different techniques of priming and cathode configurations to try and decrease the rise time, and increase the build-up of oscillations, and achieve better mode control in relativistic magnetrons. The

various techniques studied include cathode priming and magnetic priming (UM), use of the transparent cathode (UNM), and use of shaped cathodes (AFRL) [3-8].

3.2 UM's Cathode Priming

At UM the cathode priming technique was introduced in the paper "Cathode Priming of a Relativistic Magnetron" by Jones, Neculaes, Lau, Gilgenbach, and White [3]. Priming a microwave source involves some means by which the desired operating mode is preferentially excited. There are three objectives in the paper: one is faster oscillation startup, elimination of mode competition, and frequency locking. UM prepares the cathode in such a manner that its emission geometry favors excitation of the π mode. The cathodes were fabricated using projection ablation lithography (PAL) where a KrF laser etches the surface for regions of desired electron emission. For the cathode priming of a 6-cavity magnetron operating in the πmode, the cathode has three azimuthally symmetric (equally spaced) emitting regions around the cathode surface. Electron bunches form three spokes, which is inherent to operation in the π mode. Three dimensional (3D) particle-in-cell (PIC) simulations using the code MAGIC [4] show faster start-up, suppression of extraneous modes during start-up, and mode locking. UM reports that at 13.413 ns into the simulations the magnetron using cathode priming is operating in the π mode, whereas with the regular cathode the magnetron is operating in

the 2π/3 mode. The 2π/3 mode is suppressed throughout the simulations with cathode priming. UM shows that the magnetron using cathode priming is locked into the π mode, and the output frequency varies by only 20 MHz at roughly half the time as for the case using the standard cathode.

UM also invented the method of magnetic priming and in both cases they show a reduction in startup time by about 50%, which we describe next [3].

3.3 UM's Magnetic Priming

Magnetic priming, invented at UM, is studied in the paper "Magnetic Priming Effects on Noise, Startup, and Mode Competition in Magnetrons" [4]. The experiments were carried out with non-relativistic magnetrons by placing a number of small perturbing magnets on the perimeter of one of the existing annular magnets of the kW power level magnetron, providing an azimuthally varying axial magnetic field. The concept was extended to relativistic magnetrons, with 2D and 3D simulations indicating that magnetic priming significantly decreases the start time of oscillations. The 2D computational attempts were set up by imposing an axial magnetic field with three azimuthal variations to prime the π mode in the 6-vane relativistic magnetron that would model ideal conditions for magnetic priming. The maxima and minima of the magnetic fields were imposed exactly in the middle of the cavities. The simulations showed a decrease in the time to start of oscillations by a factor of three, from approximately 35 ns to 13 ns. The results also showed that mode competition between the π mode and the 2π/3 was greatly decreased in the magnetically primed magnetron. The simulation results from UM's

magnetic priming techniques resulted in a faster start up time, suppression of mode competition, and fast mode locking into the π mode [4].

3.4 UNM's Transparent Cathode

The transparent cathode was proposed as a means of decreasing the start time of oscillations in the A6 relativistic magnetron. Initial MAGIC PIC simulations revealed that, in addition to decreasing the start time of oscillations, mode competition can be eliminated, and the range of magnetic fields over which the A6 magnetron could be operated is increased for the transparent cathode when compared with the solid cathode. The paper by Schamiloglu and Fuks, "The Transparent Cathode: Rejuvenator of Magnetrons and Inspiration for New RF Sources" [5] also introduces other RF sources that could benefit from utilizing the transparent cathode, such as the ubitron, relativistic magnetron with diffraction output, and the Mitron.

The paper "Experimental Verification of the Advantages of the Transparent Cathode in a Short-Pulse Magnetron" [6] presents the results of experimental as well as simulation research conducted at UNM. The transparent cathode, which is comprised of a thin-walled hollow cylinder with periodic strips removed axially (see Fig. 1), yields performance improvement by self-consistently providing three different priming techniques: cathode priming, magnetic priming, and electrostatic priming [6].

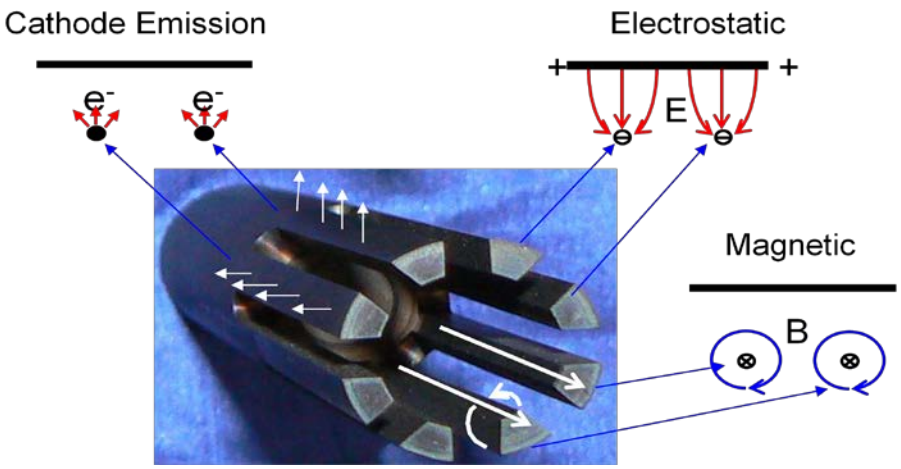

Figure 3.1. Photograph of transparent cathode with field lines showing cathode priming, electrostatic priming, and magnetic priming. [6]

Cathode priming invented at UM introduces periodic electron emitting zones around the azimuth of a solid cathode as discussed earlier. The discrete regions force electrons to bunch into the desired mode. The cathode strips in the transparent cathode act as discrete emission regions also forcing discrete electron bunching, thereby providing cathode priming. The transparent cathode also has Electrostatic priming that contributes to pre-bunching. The transparent cathode provides electrostatic priming when the electric field gains an azimuthal component around each strip this component provides a modulated field. The following figures present MAGIC simulations results carried out at UNM [6].

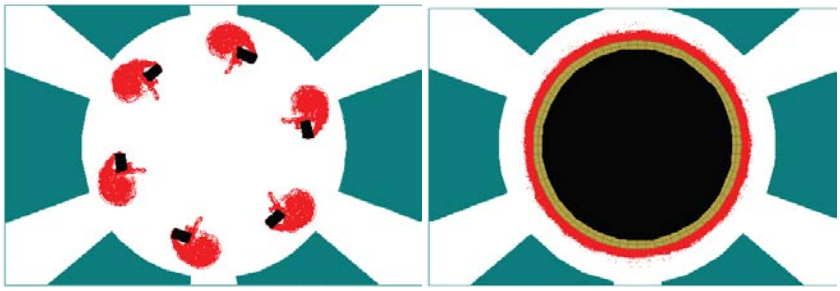

Figure 3.2. (a) Electron prebunching in the transparent cathode (in red). (b) solid ring of electrons around the solid cathode [6].

The transparent cathode also self-consistently provides magnetic priming. The axial currents along the longitudinal cathode strips produce azimuthal magnetic fields locally around the strips expressed by Ampere's Law. Magnetic priming is achieved through the periodically modulated magnetic field.

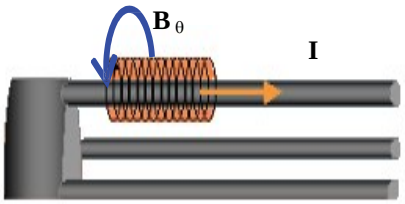

Figure 3.3. The axial current in the cathode strip and the corresponding azimuthal magnetic field lines [6].

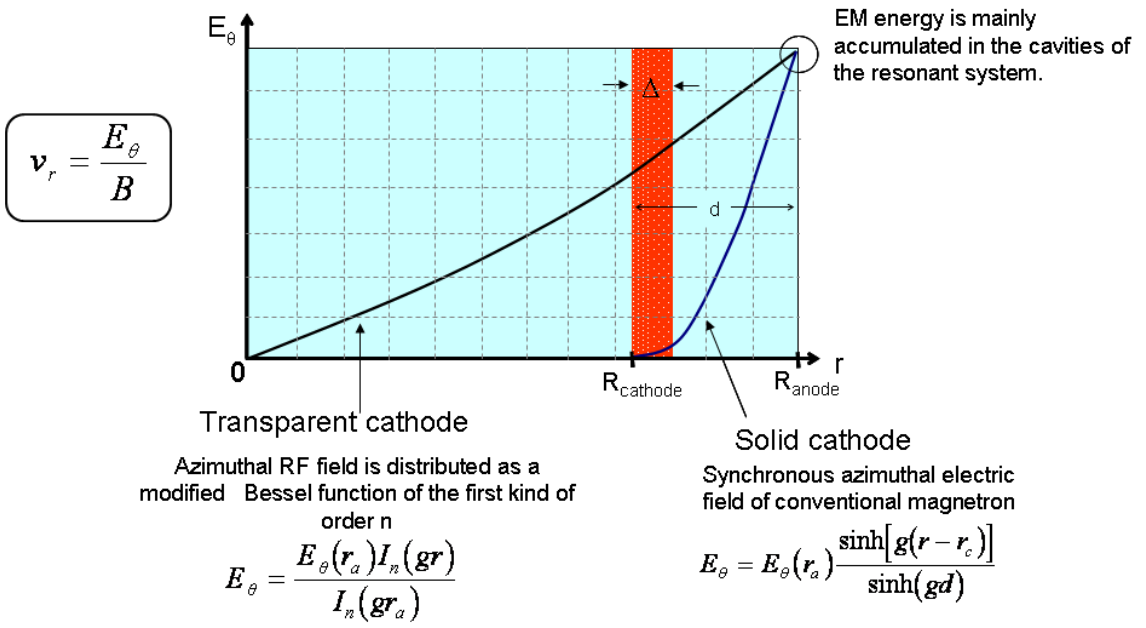

Figure 3.4. Dependence of the azimuthal electric field of the synchronous wave on radial position for a transparent cathode versus a solid cathode [6].

The transparent cathode also has the added benefit RF priming that is achieved through the higher amplitude first order wave electric field E_Θ acting on the electrons giving them a greater velocity. With a solid cathode E_Θ goes to zero on the surface of the cathode while with a transparent cathode E_Θ decreases to zero on axis. The field distribution in a magnetron with a transparent cathode provides larger field amplitude in the electron sheath region as compared to a solid cathode. This mechanism results in a larger radial velocity of the electrons and a faster rate-of-build-up of oscillations. The simulations at UNM were carried out using the PIC code MAGIC. The results will be presented later in this thesis for comparison with ICEPIC results [7].

Through the experiments and simulations the transparent cathode has self-consistently shown significant improvement of start conditions, faster rate-of-build-up of oscillations, and improvements in the output characteristics. UNM has achieved high radiated powers on the order of 1 GW, high electronic efficiency, and very stable microwave generation over a wide range of magnetic fields [5-9].

3.5 AFRL's Shaped Cathode

The paper from the AFRL group "Virtual Prototyping of Novel Cathode Designs for the Relativistic Magnetron" is where several "novel cathode" designs are discussed and studied [10]. Three cathode designs were examined: the shaped cathode, the eggbeater cathode (a UNM variation of the transparent cathode), and the original transparent cathode. The simulation work carried out by Fleming and Mardahl examined designs that would prime the magnetron to start oscillations quickly and only in the π mode. The simulation work was carried out using ICEPIC. The cathode designs were simulated using UM's magnetron anode block dimensions and AFRL's A6-3 relativistic magnetron to operate in the π mode. ICEPIC was used to simulate the entire magnetron device in 3D. This included the upstream shank region where the input voltage is introduced, the interaction region where charged particles are emitted, and the extraction ports. They examined the case for an applied voltage of 400 kV, with a 50ns voltage rise time and an axial magnetic field of 2.4 kG. The transparent cathode showed fast π mode lock-in and

dominance as well as high efficiency. Voltage scans were carried out at 2.8 and 3.2 kG and average efficiencies of 30% were achieved [10].

Chapter 4

Software Description

4.1 Importance of Simulations

Design and development of technologies hinge on the close collaboration between theory, simulation, and experiment. Computational techniques are a critical component of the research and design process, which is especially crucial for electromagnetic engineering systems where solutions to Maxwell's equations in complex geometries are difficult to solve for. In the past, advances were gained primarily through experimentation, which is expensive and time consuming. Simulation provides many benefits such as shorter turnaround time, unlimited diagnostic capabilities, and a controlled environment [11].

Computational Electromagnetics (CEM) is defined as the application and utilization of digital computers to develop and obtain numerical results for the interaction of electromagnetic fields with physical objects and their environment. The growth and development of CEM is continually changing how we interpret, formulate, and solve electromagnetic problems. CEM is also expanding the breadth and depth of the analysis and understanding of such problems solved. CEM has become a way to complement and complete the more traditional validation techniques inherent in engineering and science [11].

Verification and validation most commonly includes a comparison of multiple sets of observable data either validating measurements with computer simulations or comparing multiple simulation runs. This process is necessary to gain insight into error mechanisms, to ensure consistency, accuracy, as well as repeatability. This also helps to guide and measure the assessment of complex systems. A further step in the development of the verification and validation process is the cross-validation of multiple sets of data from differing simulation platforms to determine the degree of convergence. Also, by comparing results across multiple platforms we gain insight as errors arise and we are able to analyze these errors. We would not gain this insight if we were to only use one platform to simulate. We would argue that this technique has many benefits to the understanding of the physics, the repeatability of experiments, and the overall development of the experimental work.

4.2 Focus of Research

Simulations of the A6 magnetron with a transparent cathode using the 3D code ICEPIC at AFRL were carried out to examine the performance of the transparent cathode and compare them with the results from MAGIC simulations previously carried out at UNM. The bulk of the simulation work carried out for the transparent cathode has been using the MAGIC PIC code. Simulation is critical for the analysis and design of HPM sources. Using the well-recognized and well-developed software ICEPIC provides for an even greater analysis of the work performed at UNM. This second set of validation work has several benefits: first as, an academic exercise, to complement prior simulation work

of the transparent cathode. Second it also adds to the database of problems analyzed using ICEPIC.

4.3 Description of MAGIC

MAGIC is a fully electromagnetic, 3D particle-in-cell code self-consistent with relativistic kinematics. It utilizes a finite difference time domain solver to calculate the processes that involve interactions between space charge and electromagnetic fields. The algorithm solves the full set of Maxwell's time-dependent equations to obtain electromagnetic fields. To obtain the relativistic particle trajectories the Lorentz force equation is solved. To obtain current and charge densities the continuity equation is used. The codes in the MAGIC tool suite are built on an application independent software library [12].

4.4 Description of ICEPIC

AFRL developed ICEPIC to specifically support the development of HPM sources. In addition, ICEPIC was specifically designed from the start to run on massively parallel computer systems available to AFRL. ICEPIC is a massively parallel 3D Cartesian PIC code. ICEPIC solves Maxwell's equations and the relativistic Lorentz force law time domain with a fixed staggered grid to difference and advance, in time, Faraday's Law (Eq. (4.1)) and Ampere's Law (Eq. (4.2)) using the Yee technique[13].

$$\frac{\partial \mathbf{E}}{\partial t} = c\nabla \times \mathbf{B} - \mathbf{J} \tag{4.1}$$

$$\frac{\partial \mathbf{B}}{\partial t} = -c\nabla \times \mathbf{E} \tag{4.2}$$

The electric field **E** and current density **J** are located on the primary cells' edges while the magnetic field **B** is on the cells' faces. The fields are advanced forward in time using a leapfrog method. Momenta and positions of particles are updated via the Lorentz force law (Eq. (3.3)) using the Boris relativistic particle push. The new velocities and positions are updated by way of the leapfrog technique that has the advantage of simplicity and second order accuracy.

$$\mathbf{F} = m\frac{d\gamma \mathbf{v}}{dt} = q\left(\mathbf{E} + \frac{\mathbf{1}}{c}\mathbf{v} \times \mathbf{B}\right) \tag{4.3}$$

When new charged particles are introduced into the simulation and their position and velocity are calculated using the latest electric and magnetic field updates, a new current and charge density can be determined. These densities can then be used to calculate the new electric and magnetic fields at the grid points. Interpolating these fields to the most recent location of the particles will push particles to a new location. The process is then repeated [13].

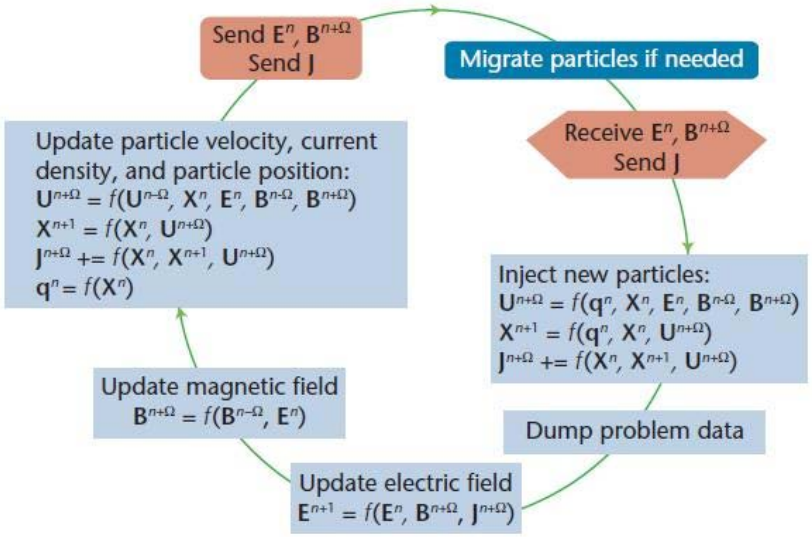

Figure 4.1. The main update loop for ICEPIC accompanied by message sends and receives [13].

Current and charge densities are evaluated from the new velocities and position using Villasenor and Buneman's charge conserving current weighting algorithm. Once the field equations, charge density, and current are updated on the grid the loop can start again. ICEPIC runs on a parallel architecture and to run efficiently uses a dynamic load balancing scheme; in this manner particles and field data can be evenly allocated between all the CPU's. This helps to alleviate heavy computational burden on one machine [13].

The transparent cathode was simulated with the A6 magnetron design, which consists of a cylindrical anode structure of axial length of 7.2 cm, anode radius of 2.11cm, and cavity radius of 4.11 cm. The cavity angular width is 20º while the vane structure is 40º. The transparent cathode is a thin walled cylindrical structure with a cathode radius of

1.58 cm and wall thickness of 2mm. The strips are periodically arranged at 60º of separation with an angular width of 10º.

4.5 Simulation Set-Up

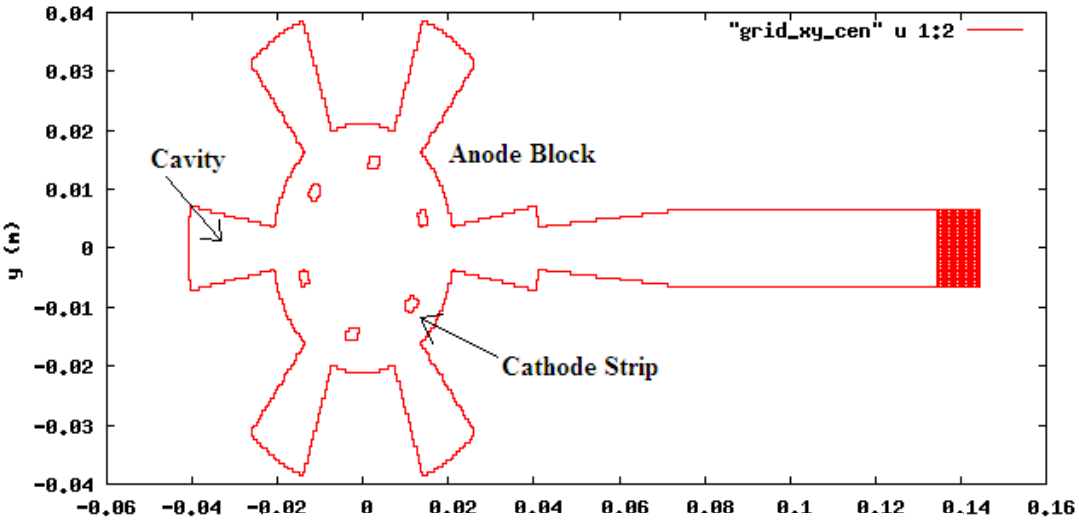

Figure 4.2. Grid plot of A6 magnetron in ICEPIC.

We use ICEPIC to simulate the A6 relativistic magnetron, which includes the entire magnetron along with the interaction region, the waveguide with a PML boundary condition where power is extracted, the cathode where particles are emitted, and the downstream cathode shank that connects to the pulsed power system. The simulations are carried out using a grid resolution of dx = 0.5 mm. The resolution of the interaction region is important for convergence of the solution. We are well resolved with an interaction region of 0.53 m and a frequency of 4.0 GHz. Studies in the literature show simulations have been performed to study convergence when analyzing the A6 driven by

a transparent cathode. The convergence studies performed previously at AFRL had shown that dx =0.75 mm for the interaction region was sufficient [13]. At a resolution of 0.5 mm our grid volume in the x-direction is 608 cells, in the y-direction 608 cells, and in the z-direction 637 cells for a total of 235,475,968 cells. Our simulations were run on 64 x 3.0 GHz Intel Woodcrest CPUs of an Advanced Technology Cluster. Each simulation took approximately 24 hours. At saturation our simulation contains approximately 16 million particles. These particles are emitted via a space-charge-limited explosive field emission algorithm. Figure (4.3) shows the electron particle plot of the A6 magnetron with transparent cathode, the wave guide for microwave extraction, and the PML. The particles are clearly in a six spoke formation indicative of the 2π-mode. For comparison Fig. 4.4 shows the electron particle plot obtained from the MAGIC simulations.

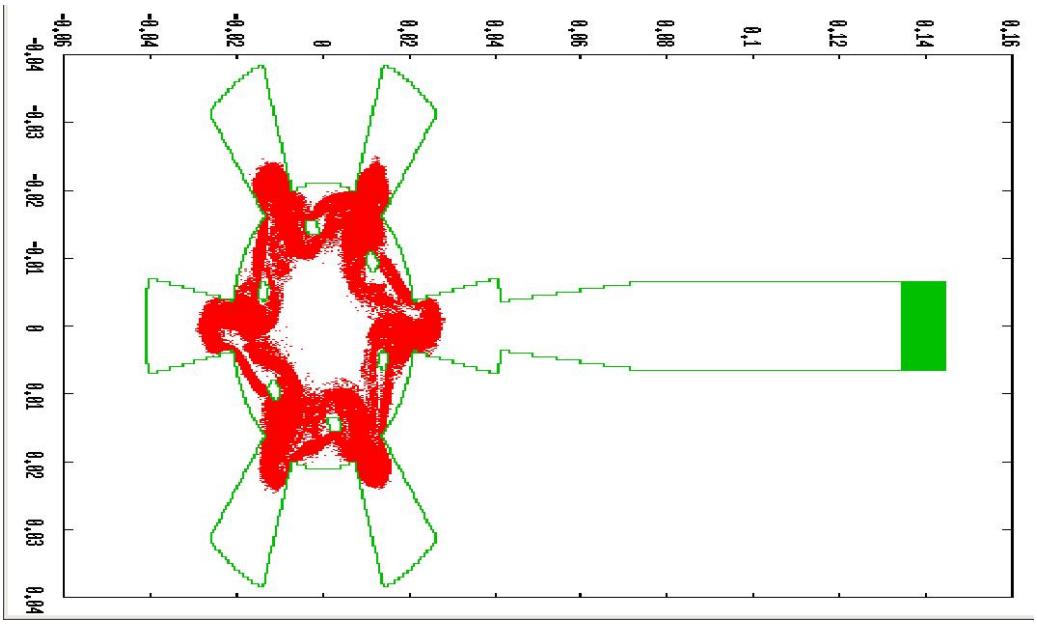

Figure 4.3. Grid plot of A6 magnetron in ICEPIC with particle emission in the 2π mode.

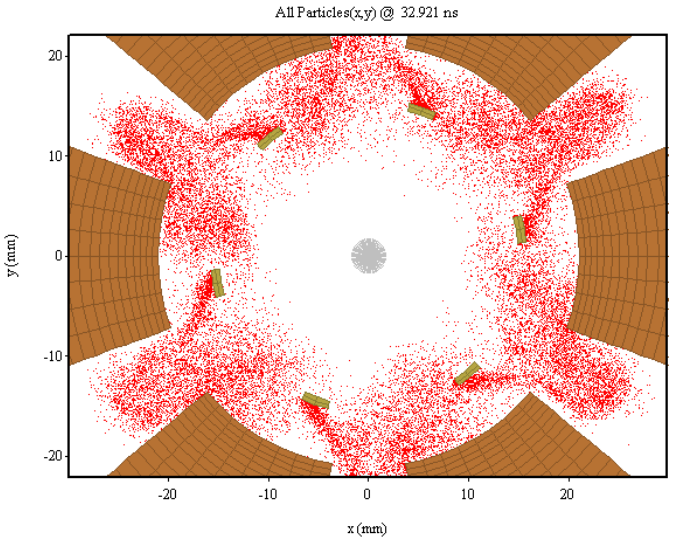

Figure 4.4 Grid plot of A6 magnetron in MAGIC with particle emission in the 2π mode.

The axial length set to emit is 10.2 cm along the z-direction at z = -0.056 m and ending at z = 0.046 m. The emission threshold was uniform across the entire surface and was set to emit when the normal electric field exceeded 2×10^7 V/m. The space-charge-limited algorithm was used such that the amount of charge emitted was sufficient to negate the electric field along the surface for each time step . A voltage signal is applied via a boundary condition on the most upstream end of the model where the pulsed power pulse forming line would be located. The pulsed power system has not been included in the simulation; rather, it is emulated by the Poisson solution. The Poisson solution establishes a potential at the boundary that then propagates down the cylinder, thus creating a diode voltage throughout the magnetron. The pulse is established as a linear 1 ns ramp followed by a constant flat top for the remainder of the simulation. The simulation runs extend to 90 ns. A uniform axial magnetic field was applied throughout to simulate the external coils used in the experiment [13].

Chapter 5

Simulation Results

5.1 ICEPIC Voltage profile

The simulations carried out at UNM using MAGIC were conducted with a constant voltage of 350 kV. When implementing a magnetic field scan MAGIC uses an algorithm that holds the voltage constant at the input port for each magnetic field imposed. ICEPIC does not possess this capability. In ICEPIC, when the Poisson solve was applied at 350 kV the voltage that was measured at the input varied due to reflections and different values of magnetic field as the simulation parameter scan proceeded. In order for us to make a direct comparison with MAGIC's results we ran numerous simulations requiring 100's of simulation hours at varying voltages and varying magnetic fields and then sampled the simulations that ran at an observed 350 kV. Many solutions were discussed to try and replicate the solutions from MAGIC as closely as possible. There are several differences in the way that MAGIC is implemented and the way ICEPIC is implemented, constant voltage, spherical coordinates vs. Cartesian, adaptive gridding, and particle density. MAGIC has the capability to implement a boundary condition that keeps voltage constant for a given port no matter what magnetic field is imposed. ICEPIC again does not possess this capability. Several different strategies were discussed and implemented to try and replicate this scenario in ICEPIC but they were

unsuccessful. It has also been discussed whether the ICEPIC team wants to have this capability. The best solution was actually the easiest solution and that was just to run several iterations with a fixed magnetic field and vary the input voltage until a final approximately 350 kV measured voltage was reached.

Another attempt was made to try and replicate the constant voltage by including the transmission line and the vacuum oil interface. This was implemented to try and give the magnetron a matched load and hopefully eradicate some of the reflections. The results yielded again similar trends. There was also a huge burden computationally on the system. Simulations that had once taken 12 hours were now taking 72 hours and longer.

The input voltage is determined by integrating the electric field radially from cathode to anode near the upstream point at which the Poisson boundary condition is applied. Figure 5.1, presents a typical ICEPIC voltage profile for a magnetic field of 0.62 T. The red line indicates a time average diode voltage of 350 kV. For comparison a typical voltage profile for MAGIC is in figure 5.2 at B = 0.62T

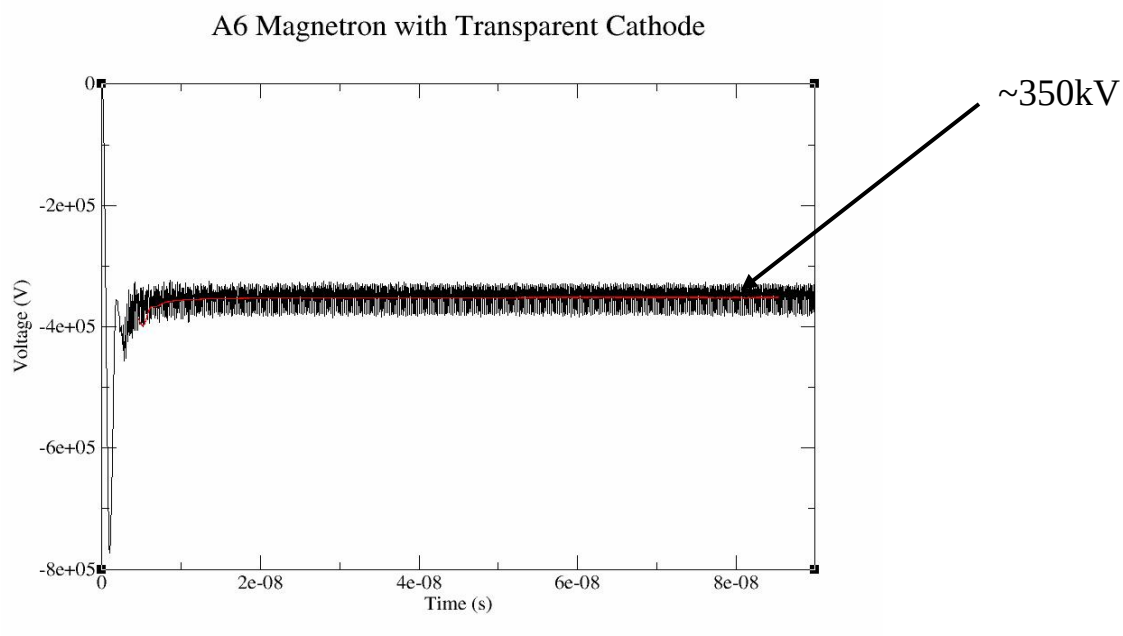

Figure 5.1. Voltage averaged over time in ICEPIC simulations (red line indicates 350kV).

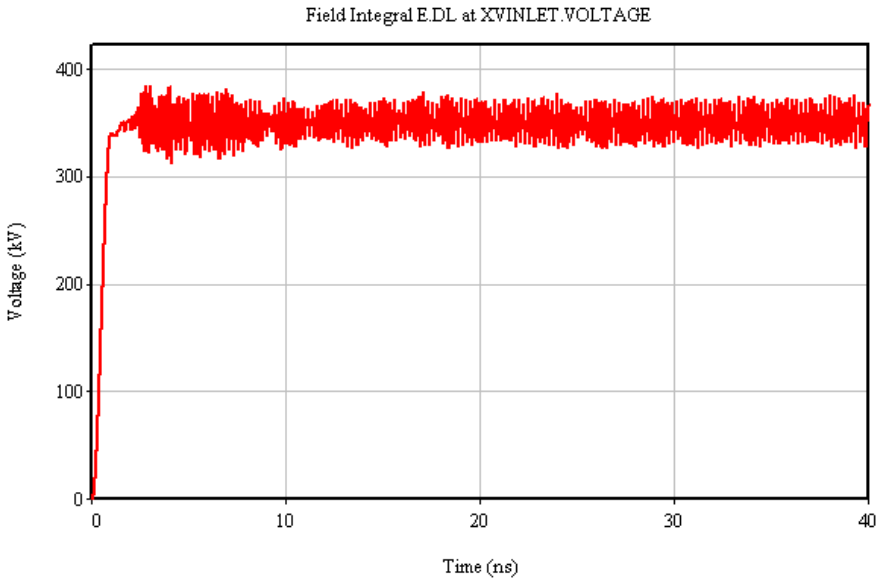

Figure 5.2. Voltage averaged over time in MAGIC simulations (red line indicates 350kV) [15].

5.2 Mode Amplitude and FFT

The time history of mode amplitudes is presented in Fig. 4.5. The time history of the voltage between each vane structure of the anode block is recorded. A fast Fourier transform (FFT) to wave-vector space is then used to extract the modes present in the interaction region. We confirm that the A6 magnetron with transparent cathode is dominated by the 2π mode at 4.0 GHz. We can also see by the figure that there is an immediate mode excitation into the 2π mode before 5 ns. Mode excitation is similar for the other high RF output power simulations.

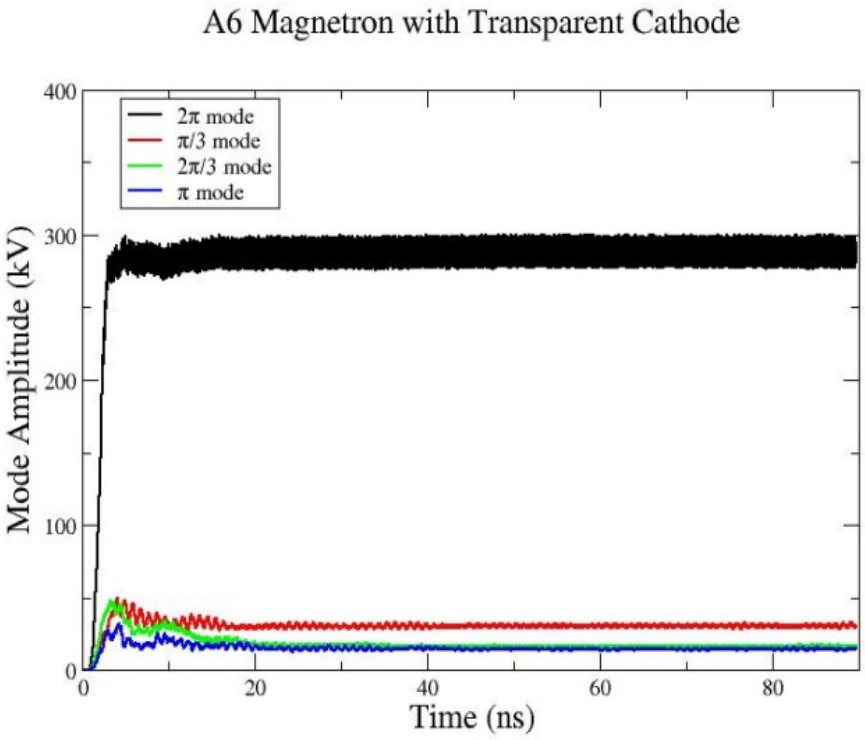

Figure 5.3. Mode amplitude plot as a function of time from ICEPIC simulations.

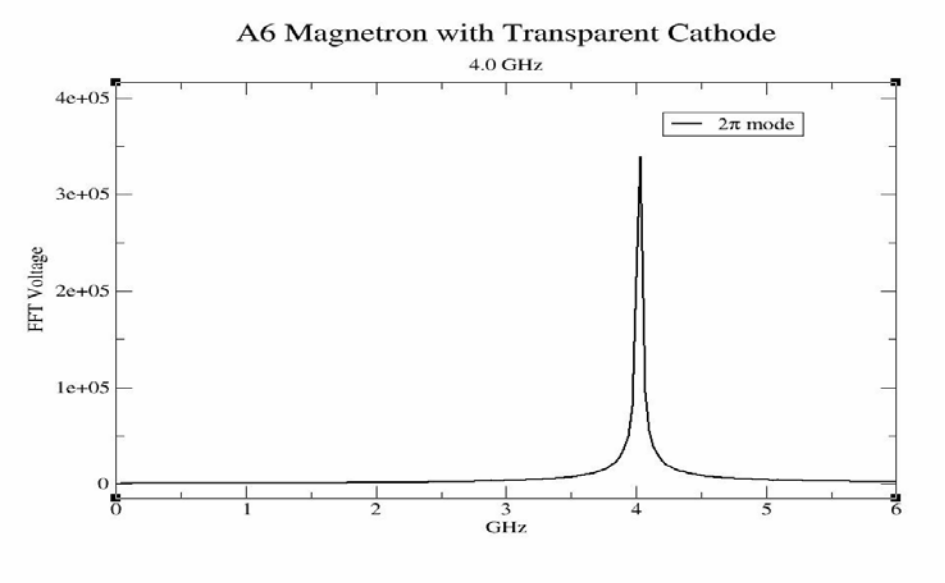

Figure 5.4. FFT from ICEPIC simulations shows clear 2π mode at 4.0 GHz.

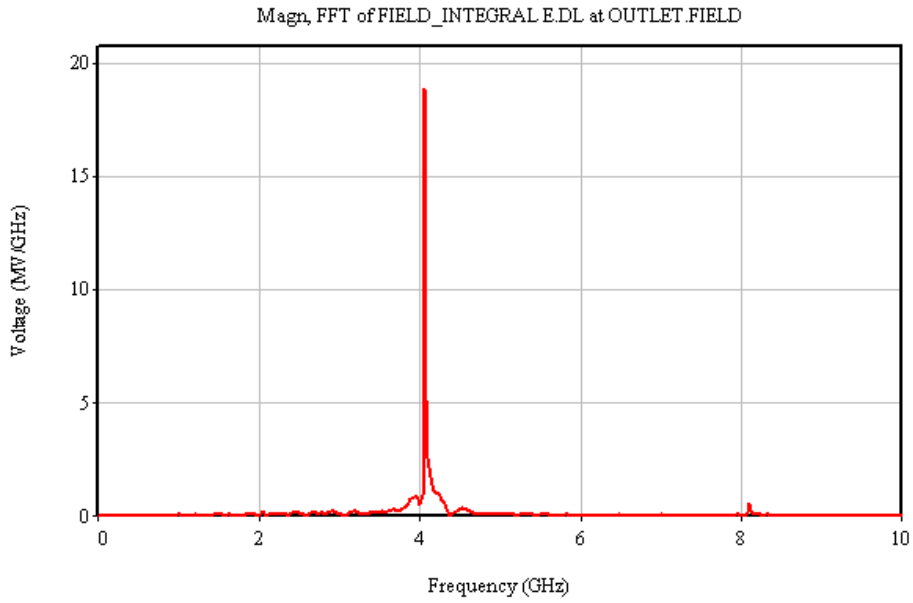

Figure 5.5. FFT from MAGIC simulations shows clear 2π mode at 4.0 GHz [15].

5.3 B-Scan/Output Power

The simulations carried out at UNM using MAGIC were conducted with a constant voltage of 350 kV. When implementing a magnetic field scan MAGIC uses an algorithm that holds the voltage constant at the input port for each magnetic field imposed. ICEPIC does not possess this capability. In ICEPIC, when the Poisson solve was applied at 350 kV the voltage that was measured at the input varied due to reflections and different values of magnetic field as the simulation parameter scan proceeded. In order for us to make a direct comparison with MAGIC's results we ran numerous simulations requiring 100's of simulation hours at varying voltages and varying magnetic fields, and then sampled the simulations that ran at an observed 350 kV. Figure 5.6 shows the range of magnetic field over which 2π mode oscillations take place at 350 kV for ICEPIC generated data. For comparison we have a similar graph (Fig. 5.7) using data points from UNM with magnetic field varying from 0.60 T to 0.68 T [15]. We have extracted RF power through a waveguide terminated with a PML. RF power is evaluated via the surface integral of the outward Poynting flux. We obtained a peak measured output power of 800 MW while MAGIC consistently obtained 1 GW. The power obtained in MAGIC and the power obtained in ICEPIC differs by about 200 MW, which is within 20% (see Figs. 5.6 and 5.7).

For magnetic fields greater than 0.66 T and at 350 kV, MAGIC continues to yield an RF output power of ~1 GW. Unlike the results from MAGIC, there is a sharp

decrease in output power beyond 0.66 T. This drop off in RF power is due to a rise in mode competition. Beyond B = 0.66 T, the 2π mode is no longer dominant.

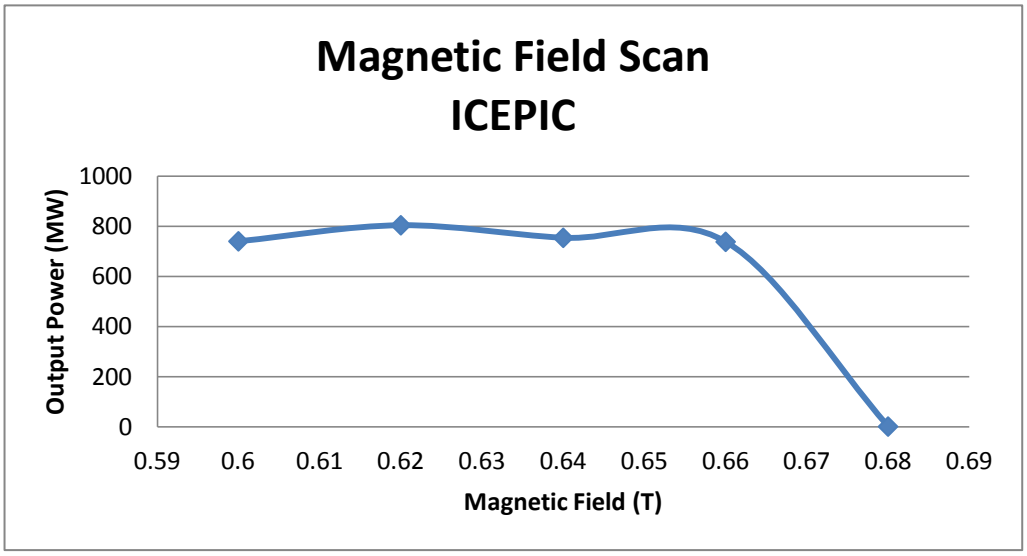

Figure 5.6. Power as a function of magnetic field obtained from the ICEPIC simulation data.

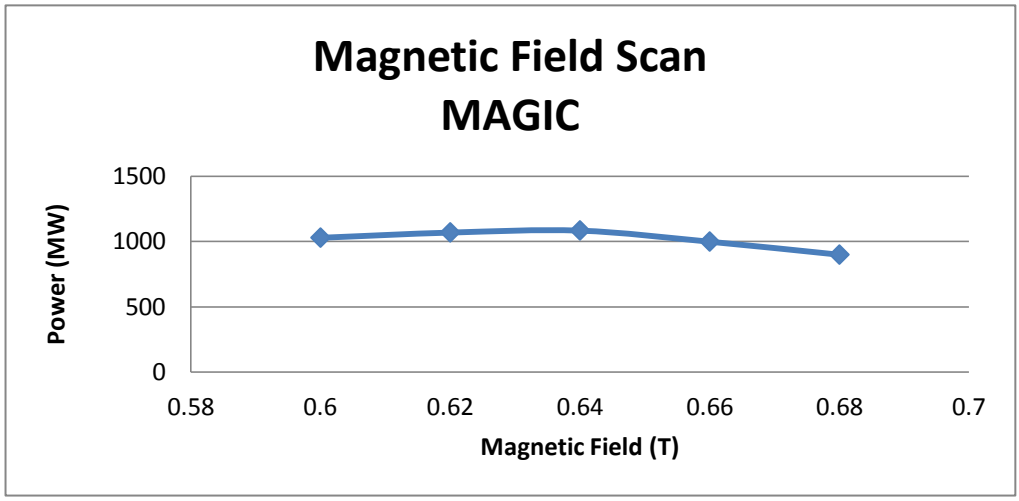

Figure 5.7. Power as a function of magnetic field obtained from the MAGIC simulation data.

To facilitate a direct comparison with MAGIC we sampled five simulations with varying magnetic field at voltage ~350 kV. The B=0.62 T simulation is chosen as a reference that typifies magnetron performance for the other simulations that successfully ran in the 2π mode. Figure 5.8 and 5.9 is a measurement of the output power as a function of time for this reference. The mean RF output power is 800 MW.

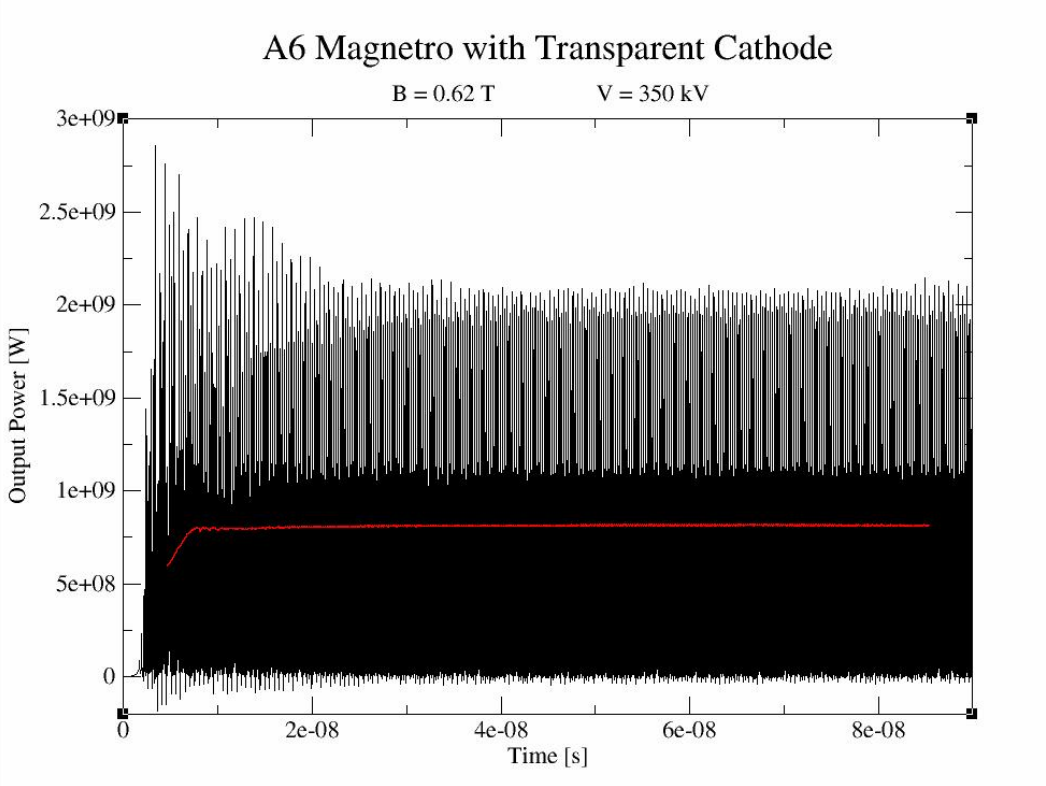

Figure 5.8. Mean RF output power is 800 MW in ICEPIC simulations.

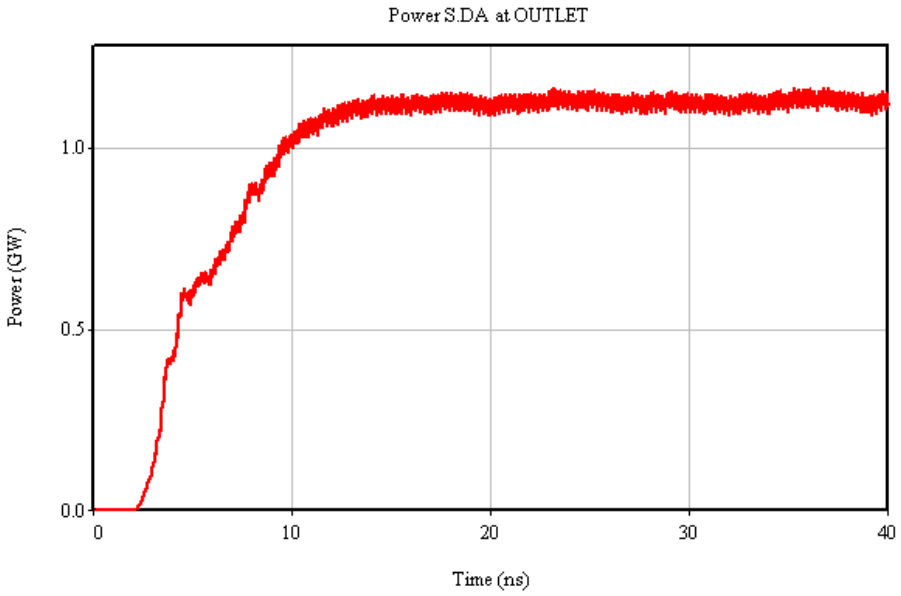

Figure 5.9. Mean RF output power is 800 MW in MAGIC simulations.

5.4 Effeciency and Current profile

Electronic efficiency for our ICEPIC model is determined by the ratio of input power to RF output power. As discussed earlier the input power is calculated as $P = I*V$, which is determined by the input current supplied to the cathode I and the input voltage V. In addition, as discussed earlier, ICEPIC uses a current diagnostic that integrates the magnetic field B around a circle to determine the total current traveling through that circle. In our simulations this is placed at the end of the chamber to determine current loss. ICEPIC also has a diagnostic that measures the time history of current that is determined by the charge passing through a surface; in our simulations this is the anode current.

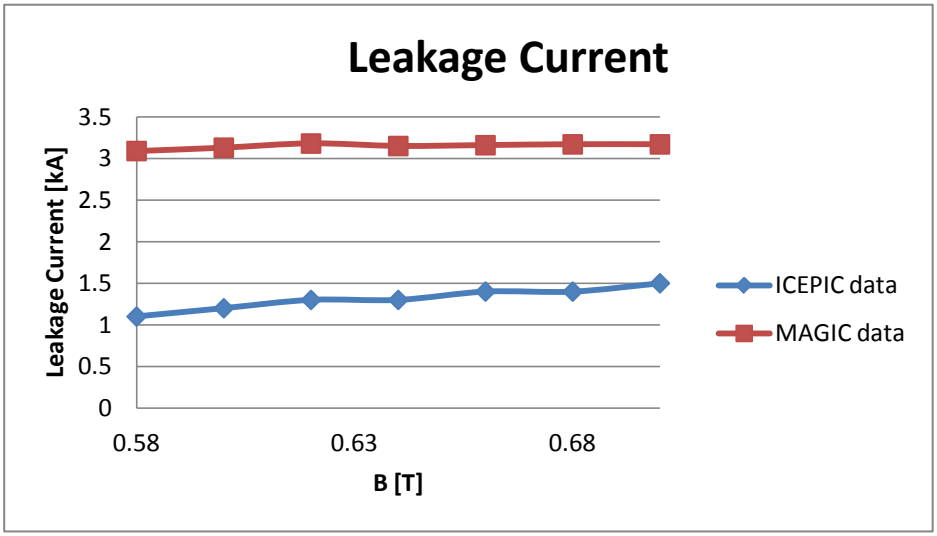

Figure 5.10. Plot of the leakage current as a function of the magnetic field for ICEPIC and MAGIC.

ICEPIC also has a diagnostic that measures the time history of current that is determined by the charge passing through a surface; in our simulation this is the anode current. The two currents together provide us with total current *I*.

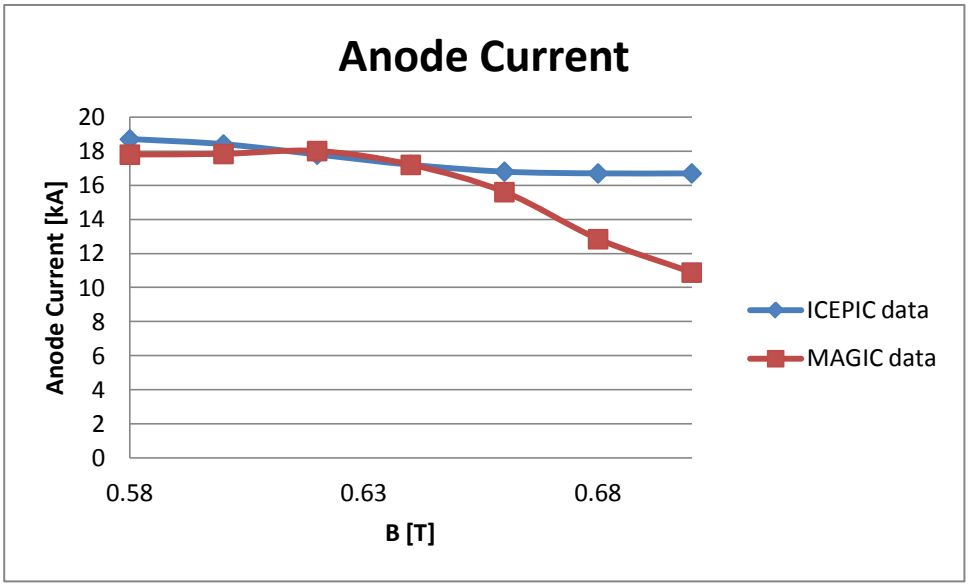

Figure 5.11. Plot of anode current as a function of magnetic field for ICEPIC and MAGIC.

The following graphs show the time history of the total current from ICEPIC simulations this includes anode current and leakage current. It is more of a system wide diagnostics. The MAGIC current profiles are the anode current and it is just differing styles of diagnostic tools.

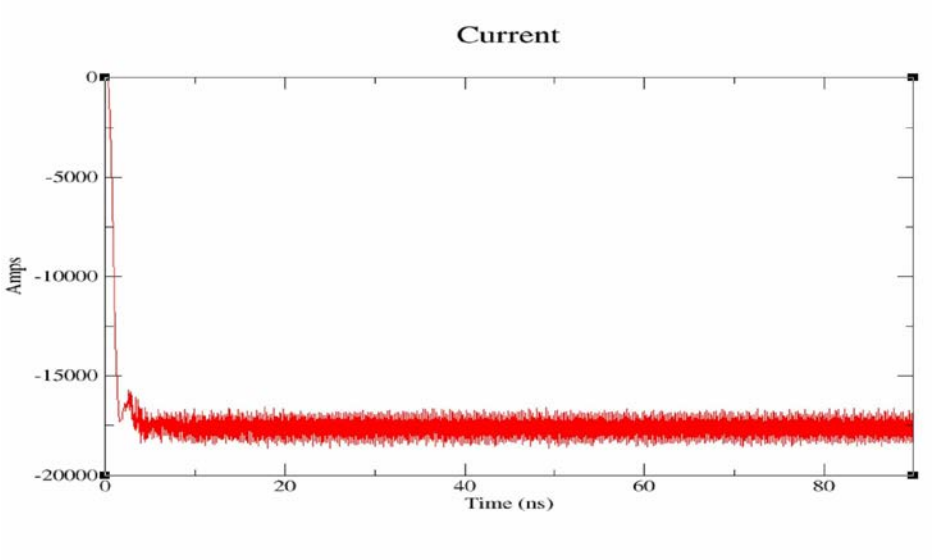

Figure 5.12. Time history of the total current profile for ICEPIC sampled data of B = 0.62 and V = 350kV.

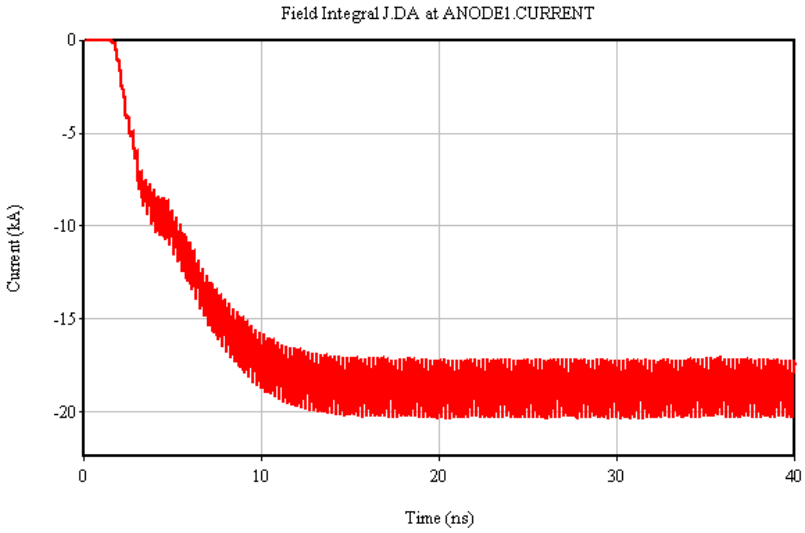

Figure 5.13. Time history of the anode current profile for MAGIC sampled data of B = 0.62 and V = 350kV.

The voltage V is the measured input voltage, discussed earlier, as the Poisson boundary condition. The reference simulation at a magnetic field of 0.62 T with a measured 350 kV voltage yields an RF output efficiency of 11.7%, which is typical of our sampled data. It is at a magnetic field of 0.68 T above which we see a sharp decline in RF output and efficiency that diverges from the results obtained in MAGIC simulations [15].

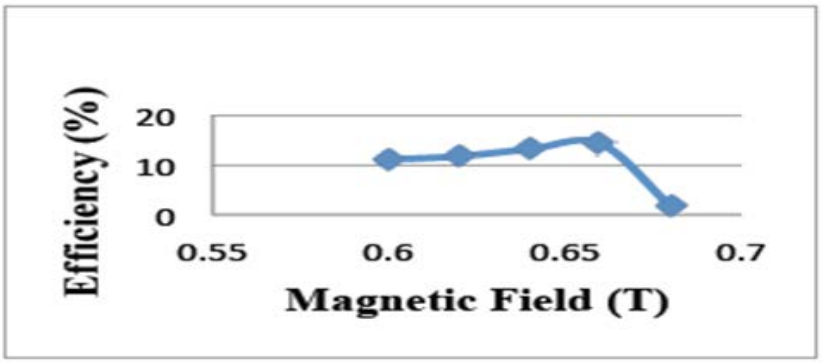

Figure 5.14. Efficiency as a function of magnetic field in ICEPIC calculated as the total efficiency with total current.

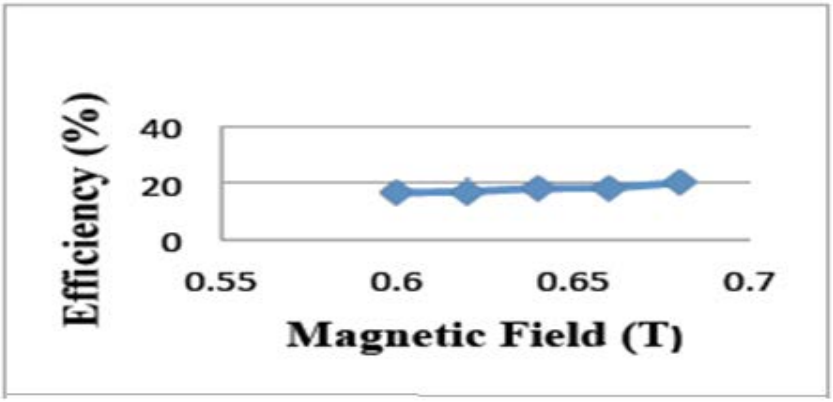

Figure 5.15. Electronic efficiency as a function of magnetic field in MAGIC.

5.5 Discussion

ICEPIC and MAGIC simulations of the A6 magnetron, driven by a transparent cathode, yielded agreement on several key magnetron performance measures such as 2π mode dominance as well as oscillations at 4 GHz. We were able to confirm that immediate spoke formation takes place and remains stable over a wide range of magnetic fields. Additionally, other research conducted by Haynes Wood with AFRL and UNM has shown good agreement between the MAGIC and ICEPIC simulations.

However, there remain several outstanding issues. ICEPIC has shown RF output power of 800 MW with efficiencies of ~12%, which has consistently remained lower than the results from MAGIC. Additionally, mode competition eradicated significant RF power output for ICEPIC simulations at a magnetic field above 0.66 T. No drop-off was observed in MAGIC simulations at 350 kV. Such a drop-off does exist in MAGIC data generated at 250 kV [15]. Additionally, it must be noted that MAGIC simulations were conducted in polar coordinates whereas the ICEPIC simulations were on a Cartesian mesh. Asymmetry associated with the stair stepping in Cartesian gridding of the magnetron may act to excite other modes in the simulation and thus bring about the power drop-off.

Indeed, this may also be the cause of the RF output power failing to reach 1 GW for all simulations examined here. Under-resolved ICEPIC simulations of the UM magnetron with transparent cathode yielded mode competition that was later eradicated upon a doubling of resolution [16]. A similar process may be at work here.

Many solutions were discussed to try and replicate the solutions from MAGIC as closely as possible. There are several differences in the way that MAGIC has been implemented and the way ICEPIC is implemented, and these have been already described. The best solution was actually the easiest solution and that was just to run several iterations with a fixed magnetic field and vary the input voltage until a final 350 kV measured voltage was reached. This was verified a second time and the following data is a summary of the simulations. Figures 5.8-5.13 present results for the power, anode current, and leakage current as a function of the magnetic field. The trends were exactly the same as in the simulations performed at AFRL. Another attempt was made to try and replicate the constant voltage by including the transmission line and the vacuum oil interface. This was implemented to try and give the magnetron a matched load and hopefully eradicate some of the reflections. The results once again yielded similar trends. There was also a tremendous burden computationally on the system. Simulations that had once taken 12 hours were now taking 72 hours and longer. Table 5.1 summarizes key similarities and differences between ICEPIC and MAGIC.

Table 5.1 Key parameters for ICEPIC and MAGIC

Parameters	ICEPIC	MAGIC
Coordinate System	**Cartesian (X, Y, Z)**	**Polar (r, z, phi)**
Meshing Technique	**Uniform**	**Adaptive**
Cell Resolution in Interaction Space	**Z = 0.5 mm** **X = 0.5 mm** **Y = 0.5 mm**	**z = 9mm** **r = 0.5 mm** **$\theta = 5^{o}$**
Total Number of Cells	**235 million**	**94,350**
Total Number of Particles	**16 million**	**1 million**
Basic Algorithm	**FDTD (Parallel)**	**FDTD**
Number of CPU's	**64 (3 GHz)**	**1 (3.2 GHz)**

Chapter 6

Summary and Future Work

A weakness of the A6 relativistic magnetron, with solid cathode, for applications that require short pulse high peak power is the long start time for oscillations. To address this weakness UNM has invented the transparent cathode which by design decreases the start time of oscillation, eliminates mode competition, and increases the range of magnetic fields over which the A6 magnetron can be operated. The transparent cathode achieves this by self consistently providing cathode priming and magnetic priming.

Utilizing ICEPIC for simulations we were able to ensure consistency, accuracy, and repeatability across two simulation platforms, MAGIC and ICEPIC. This multiple platform comparison also increases the breadth of validation executed at UNM and AFRL. Many hundreds of hours of simulation work was carried out to ensure that both the simulations conducted in MAGIC and also in ICEPIC were as close of a match as possible. Although we did not have the original input deck for the MAGIC simulations we used the published data to facilitate the comparison. The ICEPIC geometry was a match to the MAGIC geometry. The grid resolution, in ICEPIC, was at dx = 0.5 mm with a total cell volume of 235,475,968. The simulations were conducted on 64 CPUs which took approximately 24 hours per simulation. Particles were emitted via field emission at saturation of 16 million particles. The A6 magnetron with transparent cathode clearly preferred 2π mode at 4.0GHz which is in agreement with MAGIC. The input voltage was 350kV and simulation runs were 90ns with a 1ns rise time. The input current was 18kA and leakage current was nominal at ~1kA. Suggestions for future work should be to

conduct ICEPIC simulations in cylindrical coordinate system. The reason for this is when ICEPIC generates the grid plot in Cartesian coordinates there is some stair stepping going on around the edges. These edges may excite modes and could explain the lower output power for ICEPIC. The reason this was not carried out is ICEPIC's cylindrical coordinates system is not fully tested at this point. Another suggestion would to vary the particle count in MAGIC the particles count was ~1 million particles for ICEPIC we had ~16 million particles. It has been suggested by my mentor that maybe the particle density is too high and this could be leading to mode competition. We had lowered the particle count previously for another simulation but this resulted in lack of oscillations. The third recommendation for future work would be to compare the ICEPIC simulations with results from experiments. UNM is in the process of building an accelerator that will operate at 350kV.

REFERENCES

[1] James E. Brittain, "The Magnetron and the Beginnings of the Microwave Age," *Physics Today, 38(7), 60 (1985); doi:10.1063/1.880982*

[2] A. Palevsky, "*Generation of Intense Microwave Radiation By The Relativistic e-Beam Magnetron (Experimental and Numerical Simulation,"* Ph.D. Dissertation, Massachusetts Institute of Technology (1980).

[3] M.C. Jones, V.B Neculaes, Y.Y. Lau, R.M. Gilgenbach, W.M. White, "Cathode Priming of a Relativistic Magnetron," *Appl. Phys. Lett.,* vol. 85, pp. 6332-6334 (2004).

[4] V.B. Neculaes, M.C. Jones, R.M. Gilgenbach, Y.Y. Lau, J.W. Luginsland, B.W. Hoff, W. White, N.M. Jordan, P. Pengvanich, Y. Hidaka, and H. Bosman, "Magnetic Priming Effects on Noise, Startup, and Mode Competition in Magnetrons," *IEEE Trans. Plasma Sci.*, vol. 33, pp. 94-102 (2005).

[5] E. Schamiloglu and M.I. Fuks, "The Transparent Cathode: Rejuvenator of Magnetrons and Inspiration for New RF Sources," High Power RF Technologies, IET Conference on pp. 1-5 (2009).

[6] S. Prasad, M. Roybal, J. Buchenauer, K. Prestwich, M. Fuks, E. Schamiloglu, "Experimental Verification of the Advantages of the Transparent Cathode in a Short-Pulse Magnetron," *Pulsed Power Conference, 2009. PPC '09. IEEE* 10.1109/PPC.2009.5386242
Publication Year: 2009 , Page(s): 1 - 23.

[7] M. Fuks and E. Schamiloglu, "Rapid Start of Oscillations in a Magnetron with Transparent Cathode." *Phys. Rev. Lett.*, vol. 95, pp. 205101-1-4 (2005).

[8] H.L. Bosman, M.I. Fuks, S. Prasad, and E. Schamiloglu, "Improvement of the Output Characteristics
of the Magnetrons using the Transparent Cathode," *IEEE Trans. Plasma Sci.*, vol. 34, pp. 606-619 (2006).

[9] S. Prasad, M.I. Fuks, K. Prestwich, C.J. Buchenauer, and E. Schamiloglu, "Experimental Observation of Fast Start of Oscillations in Short-Pulse Magnetron Driven by a Transparent Cathode," *Appl. Phys. Lett.* (in preparation).

[10] T. Fleming, P. Mardahl, L. Bowers, K. Cartwright, M. Bettencourt, and M. Howers, "Virtual Prototyping of Novel Cathode Designs for the Relativistic Magnetron," *IEEE Comput. Sci. Eng.*, vol. 9, pp. 18-28 (2007).

[11] Edmund K. Miller, "A Selective Survey of Computational Electromagnetics," *IEEE Trans. On Antennas and Propagation,* vol. 36, NO. 9, (1988).

[12] Larry Ludeking, David Smithe, Mike Betternhausen, Scott Hayes, MAGIC's User's Manual, Mission Research Corp.

[13] T.P. Fleming, M.R. Lambrecht, and K.L. Cartwright, "Numerical Simulations of a Relativistic Inverted Magnetron," *IEEE Trans. Plasma Sci.*, vol. 38, pp.156-1573 (2010).

[14] T.P. Fleming, P.J. Mardahl, "Performance Improvements in the Relativistic Magnetron: The Effect of DC Field Perturbations," *IEEE Trans. Plasma Sci.*, vol. 37, pp. 2128-2138 (2009).
[15] S. Prasad, priv. comm., 2011.
[16] T. Fleming, priv. comm., 2011.